

Loss tangent fluctuations due to two-level systems in superconducting microwave resonators

A. Vallières,^{1,2} M. E. Russell,³ X. You,² D. A. Garcia-Wetten,⁴ D. P. Goronzy,⁴ M. J. Walker,⁴ M. J. Bedzyk,^{3,4} M. C. Hersam,^{4,5,6} A. Romanenko,² Y. Lu,² A. Grassellino,² J. Koch,^{3,7} and C. R. H. McRae^{8,9,10}

¹⁾Graduate Program in Applied Physics, Northwestern University, Evanston, IL 60208, USA

²⁾Fermi National Accelerator Laboratory, Batavia, IL 60510, USA

³⁾Department of Physics and Astronomy, Northwestern University, Evanston, IL 60208, USA

⁴⁾Department of Materials Science and Engineering, Northwestern University, Evanston, IL 60208, USA

⁵⁾Department of Chemistry, Northwestern University, Evanston, IL 60208, USA

⁶⁾Department of Electrical and Computer Engineering, Northwestern University, Evanston, IL 60208, USA

⁷⁾Center for Applied Physics and Superconducting Technologies, Northwestern University, Evanston, IL 60208, USA

⁸⁾Electrical, Computing and Energy Engineering Department, University of Colorado, Boulder, CO 80309, USA

⁹⁾Department of Physics, University of Colorado, Boulder, CO 80309, USA

¹⁰⁾National Institute of Standards and Technology, Boulder, CO 80305, USA

(*Electronic mail: andrevallieres2027@u.northwestern.edu)

(Dated: 7 December 2024)

Superconducting microwave resonators are critical to quantum computing and sensing technologies. Additionally, they are common proxies for superconducting qubits when determining the effects of performance-limiting loss mechanisms such as from two-level systems (TLS). The extraction of these loss mechanisms is often performed by measuring the internal quality factor Q_i as a function of power or temperature. In this work, we investigate large temporal fluctuations of Q_i at low powers over periods of 12 to 16 hours (relative standard deviation $\sigma_{Q_i}/Q_i = 13\%$). These fluctuations are ubiquitous across multiple resonators, chips and cooldowns. We are able to attribute these fluctuations to variations in the TLS loss tangent due to two main indicators. First, measured fluctuations decrease as power and temperature increase. Second, for interleaved measurements, we observe correlations between low- and medium-power Q_i fluctuations and an absence of correlations with high-power fluctuations. Agreement with the TLS loss tangent mean is obtained by performing measurements over a time span of a few hours. We hypothesize that, in addition to decoherence due to coupling to individual near-resonant TLS, superconducting qubits are affected by these observed TLS loss tangent fluctuations.

In superconducting circuits, microwave resonators are implemented for many purposes, including qubit readout,^{1,2} quantum memory,³ and quantum sensing.⁴ Superconducting microwave resonators have also become essential in characterizing losses in superconducting circuits with the goal of making higher coherence qubits^{5–10}. Measuring the intrinsic quality factors Q_i of resonators at different powers and temperatures enables the separation of the total loss into contributions from two-level systems (TLS), equilibrium quasiparticles (QP), and other loss sources such as radiation or coupling to parasitic modes^{11,12}.

Although there has been significant effort to characterize frequency fluctuations in resonators^{13–20}, the same cannot be said for fluctuations in dissipation, especially for distributed-element resonators over long time scales. While Ref. 21 measures resonator dissipation over long time scales, we expand this line of inquiry to describe how Q_i fluctuations arise from variations in the TLS loss tangent. This is evidenced by our observations of fluctuations decreasing at higher powers and temperatures, consistent with TLS saturation. We report quality factor fluctuations at low power with relative standard deviation σ_{Q_i}/Q_i of 13% in distributed-element superconducting resonators across multiple resonators, chips and cooldowns. We analyze the impacts of these fluctuations on the results of common methods of TLS loss tangent extraction.

In the case of qubits, it is becoming standard to report statistics of T_1 rather than a single value since it is known that the

relaxation time T_1 can substantially fluctuate over time^{22–26}. Similarly, we demonstrate with resonators that rapidly measuring over a few hours appropriately captures the TLS loss tangent mean and standard deviation, while performing time-averaged measurements for the same time frame represents well the mean but does not capture the width of the distribution.

All measured resonators are Nb on Si coplanar waveguide quarter-wavelength resonators inductively coupled to a feedline (see Appendix A for more information). The measurement chain consists of a vector network analyzer (VNA) to perform transmission (S_{21}) measurements across the samples, a Josephson parametric amplifier (JPA) used at lower powers, and suitable attenuators, filters, isolators and additional amplifiers for achieving desirable signal quality in the 4 GHz to 8 GHz range (see Appendix B). The transmitted signal is analyzed using a circle fit routine^{27,28} to extract Q_i and the resonance frequency f_r following

$$S_{21}(f) = Ae^{-i2\pi f\tau} \left(1 - \frac{(Q/|Q_c|)e^{i\phi}}{1 + 2iQ(f/f_r - 1)} \right), \quad (1)$$

where A is the (complex) attenuation of the line and τ is the line delay. The internal quality factor Q_i is obtained from the loaded Q and complex coupling quality factor $Q_c = |Q_c|e^{-i\phi}$ using $1/Q_i = 1/Q - \cos\phi/|Q_c|$, where the angle ϕ accounts for the impedance mismatch between the feedline and the resonator. Obtaining Q_i this way, we are able to independently

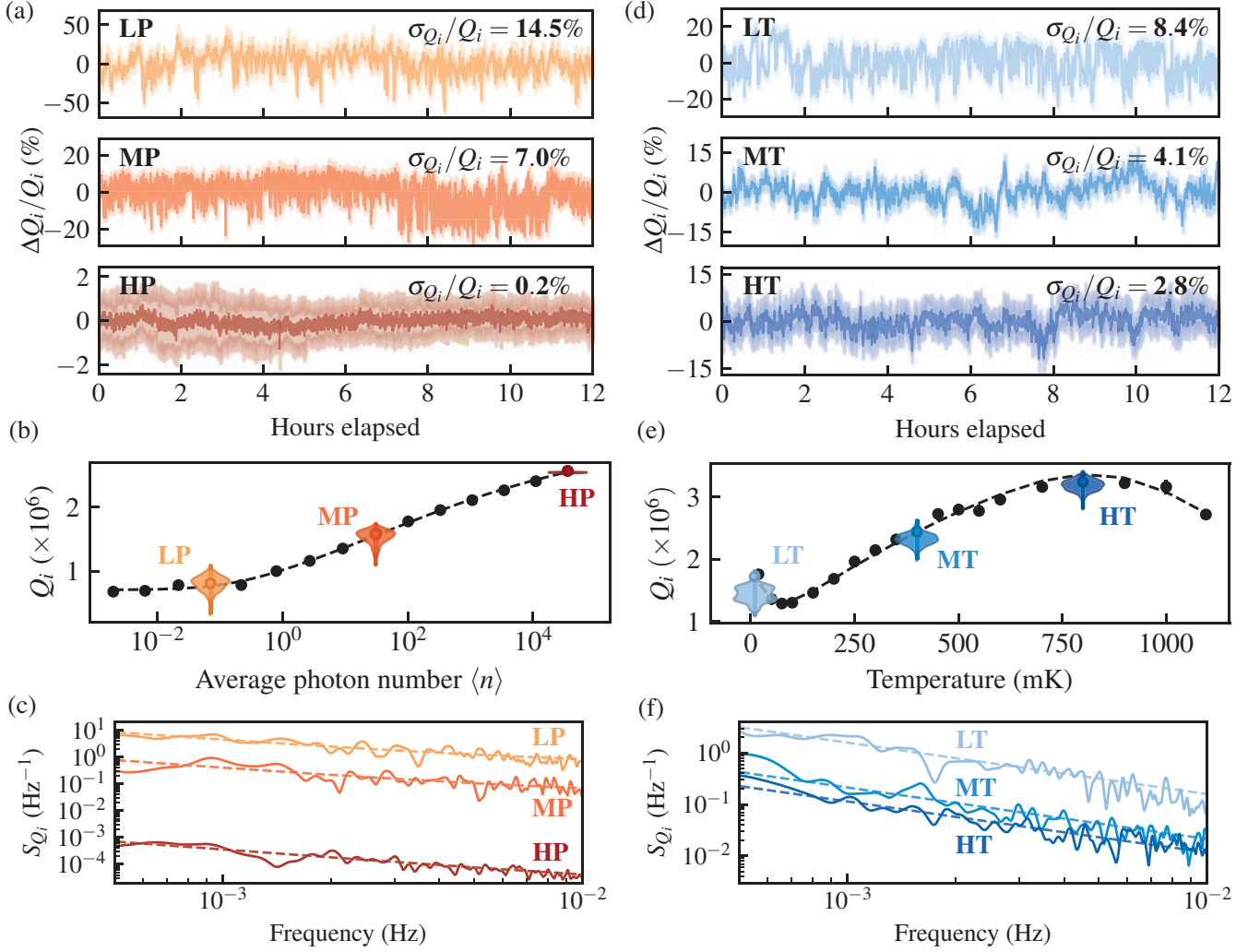


FIG. 1. Internal quality factor fluctuations with varying power (a-c) and temperature (d-f). Measurements for (a-c) were performed at base temperature (~ 10 mK) and at three different powers: low (LP, -75 dBm), medium (MP, -60 dBm), and high (HP, -25 dBm). (a) Time traces of the relative deviation from the mean $\Delta Q_i/Q_i$, showing decreasing fluctuations with increasing power, consistent with TLS saturation. The semi-transparent regions represent fitting uncertainty. (b) The three powers are represented on the TLS loss model curve with a fit to Eq. (2) shown as a dashed line. The violins show the density curves of the time traces in (a) and additionally provide a visual comparison of the fluctuation magnitudes at different powers. (c) Low-frequency noise spectra S_{Q_i} further demonstrating a decrease in fluctuations with increasing power. Notably, we observe a difference of four orders of magnitude between low and high powers. Fits to $1/f$ spectra are also shown as dashed lines to serve as guides to the eye. (d-f) Quality factor fluctuations at a power of -55 dBm at the VNA and three different temperatures: low (LT, 10 mK), medium (MT, 400 mK), and high (HT, 800 mK). In (d), we show the time traces of the relative deviation from the mean at these temperatures. We observe decreasing fluctuations at higher temperatures, also consistent with TLS saturation. The semi-transparent regions represent fitting uncertainty. We choose the temperatures in relation to TLS saturation levels as described by the model in Ref. 12; the fit is shown as a dashed line in (e). The TLS-dominated and QP-dominated regimes are shown below and above ~ 800 mK, respectively. The violins again correspond to the density curves for the traces in (d). The vertical lines at each black point correspond to fitting uncertainty of individual measurements. (f) Low-frequency noise spectra S_{Q_i} for the three temperatures, further demonstrating decreasing fluctuations with increasing temperature. Fits to $1/f$ spectra are again represented as dashed lines to serve as guides to the eye. We note that in this figure, we used two representative resonators: one for the power dependence results and another for the temperature dependence results.

measure the fluctuations of f_r and Q_i .

In Fig. 1, we explore the dependence of Q_i fluctuations on power and temperature. We observe a systematic decrease of fluctuations at higher powers and temperatures. This aligns with the idea that the fluctuations are caused by TLS: namely when TLS become saturated at high powers and temperatures,

they contribute less to the total loss^{21,29}. We note that these results hold for all resonators measured as part of this study (see Appendix H).

The analysis of the power dependence is based on a TLS

saturation model^{10,11,19,30}, according to which:

$$\frac{1}{Q_i} = \frac{1}{Q_{\text{TLS}}(n, T)} + \frac{1}{Q_{\text{PI}}} \quad (2)$$

$$= F\delta_{\text{TLS}}^0 \frac{\tanh \frac{\hbar\omega_r}{2k_B T}}{\left(1 + \frac{\langle n \rangle}{n_c}\right)^\beta} + \frac{1}{Q_{\text{PI}}}.$$

Here, F is the filling factor, δ_{TLS}^0 ($Q_{\text{TLS}}(n, T)$) the intrinsic TLS loss tangent (quality factor), ω_r the angular resonance frequency of the resonator, k_B the Boltzmann constant, T the temperature, $\langle n \rangle$ the average photon number in the resonator, n_c the critical photon number, β an empirical parameter describing TLS interaction, and $1/Q_{\text{PI}}$ represents the power-independent loss. This model is used to obtain the effective TLS loss tangent $F\delta_{\text{TLS}}^0$ from a fit of Q_i versus $\langle n \rangle$. It also informs our choice of powers to investigate fluctuations at different levels of TLS saturation.

Fig. 1(a) shows 12-hour time traces of Q_i for measurements at low (LP), medium (MP), and high (HP) powers, corresponding to -75 dBm, -50 dBm and -20 dBm at the VNA, respectively. We observe considerable fluctuations, especially at low power where Q_i varies by as much as 37% from the average during the 12 hours. We further illustrate the fluctuations' magnitude in Fig. 1(b) relative to the TLS loss model curve (S curve). Additionally, we characterize the fluctuations in the frequency domain by plotting the spectral density of the normalized Q_i time series $(Q_i(t) - \langle Q_i \rangle) / \langle Q_i \rangle$ estimated using Welch's method³¹. Here, $\langle Q_i \rangle$ refers to the average value of the time trace. We observe that fluctuations at high power are reduced by as much as four orders of magnitude compared to low power.

The temperature dependence measurements were performed and analyzed in a similar fashion. We choose temperatures relative to TLS saturation levels based on our measurements of Q_i and the model described in Ref. 12. This model explains $Q_i(T)$ by accounting for temperature-dependent TLS saturation and QP loss. Fig. 1(d) shows 12-hour time traces of Q_i at low (LT), medium (MT), and high (HT) temperatures, corresponding to 10 mK, 400 mK, and 800 mK, respectively. We observe decreasing fluctuations with increasing temperature, with an order of magnitude difference between LT and HT as shown in Fig. 1(f). These results, along with those from power dependence measurement, support the claim that the large fluctuations at low power and temperature are caused by TLS.

We further study correlations in fluctuations at different powers by performing fast interleaved measurements over 16 hours at LP, MP, and HP. We used a JPA for the lower two powers to achieve average measurement times of 38 s and 9 s per point versus 10 s for the high power measurements. The results notably show that the LP-MP pair exhibits strong correlations, in terms of both their temporal behavior and magnitude (see Fig. 2). This is consistent with a saturable loss process, such as that associated with TLS. Namely, we expect correlations between Q_i measurements at low and medium power, as TLS is the main source of fluctuations and the dominant loss channel at both power levels. This is further il-

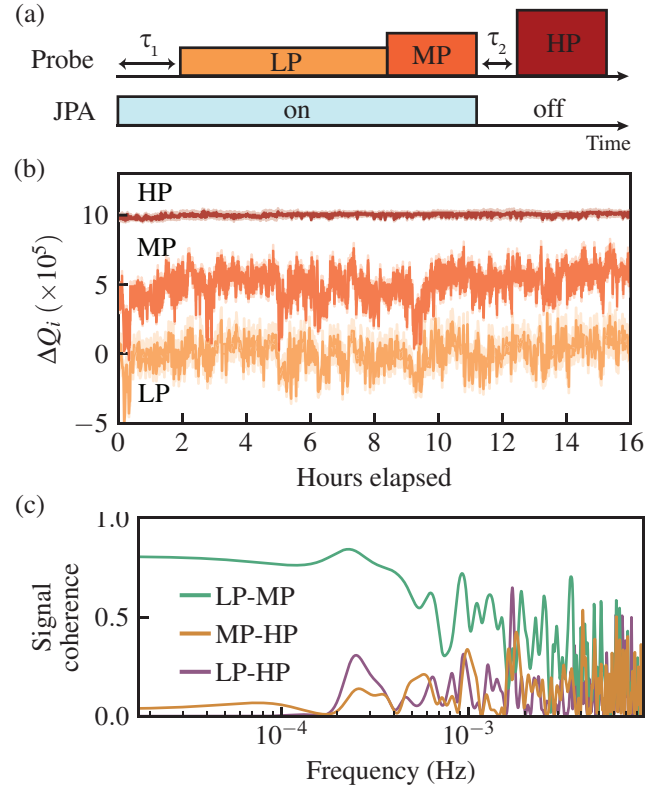


FIG. 2. Interleaved power measurements of the Q_i deviation from the average $\Delta Q_i = Q_i - \langle Q_i \rangle$ at base temperature (~ 10 mK). (a) Measurement sequence for interleaved measurements, with the JPA turned off during high-power measurements. Idling times of $\tau_1 = 3$ s and $\tau_2 = 0.5$ s were found to be sufficient to ensure that the JPA is stable when performing measurements. This sequence is repeated over 16 hours. (b) Time traces at low (LP, -75 dBm), medium (MP, -55 dBm), and high (HP, -15 dBm) powers. The MP and HP traces are shifted in ΔQ_i by 5 and 10 for better distinction. (c) The relationship between interleaved measurements at different powers is illustrated using the signal coherence (i.e., normalized cross-spectral density) for each pair of powers. Focusing on low frequencies, the LP-MP pair shows greater correlation compared to LP-HP as the source of fluctuations at low and higher powers is different due to TLS saturation. The MP-HP pair similarly exhibits little coherence for the same reason.

lustrated with the normalized cross-spectral density, or signal coherence (see Appendix E), showing strong correlation for the LP-MP pair especially at low frequencies. On the other hand, we observe practically no correlations for LP-HP at low frequencies since they are dominated by separate dissipation channels.

With the same interleaved measurements, we additionally track the effective TLS loss tangent $F\delta_{\text{TLS}}^0$ from the quality factors at low (Q_{LP}) and high (Q_{HP}) powers using $F\delta_{\text{TLS}}^0 \simeq 1/Q_{\text{LP}} - 1/Q_{\text{HP}}$ (see Fig. 3). This expression holds for low temperatures ($\hbar\omega \gg k_B T$ in Eq. (2)) and for powers within the two plateaus of the S curve. We observe large variations of $F\delta_{\text{TLS}}^0$ with $F\delta_{\text{TLS}}^0 = (9.0 \pm 2.2) \times 10^{-7}$. We further illustrate the temporal variations of the loss by plotting the approximate

S curves at different time instances (as indicated by the arrows). We note that Q_{HP} roughly stays fixed in time while Q_{LP} varies significantly between 3.3×10^5 and 1.0×10^6 . Fig. 3(c) shows that the distribution of $F\delta_{\text{TLS}}^0$ is wide and has a pronounced tail toward lower loss values. We notice that the logarithm of the data appears normally-distributed. We perform a fit to a log-normal distribution and observe good agreement. By further investigating how the sample distribution depends on measurement time (Appendix F), we find that low power measurements over a few hours should be sufficient to estimate the average TLS loss tangent with reasonable accuracy. However, averaging for such long times would inevitably result in the inability to characterize the width of the distribution, which may be of interest in materials study, for example.

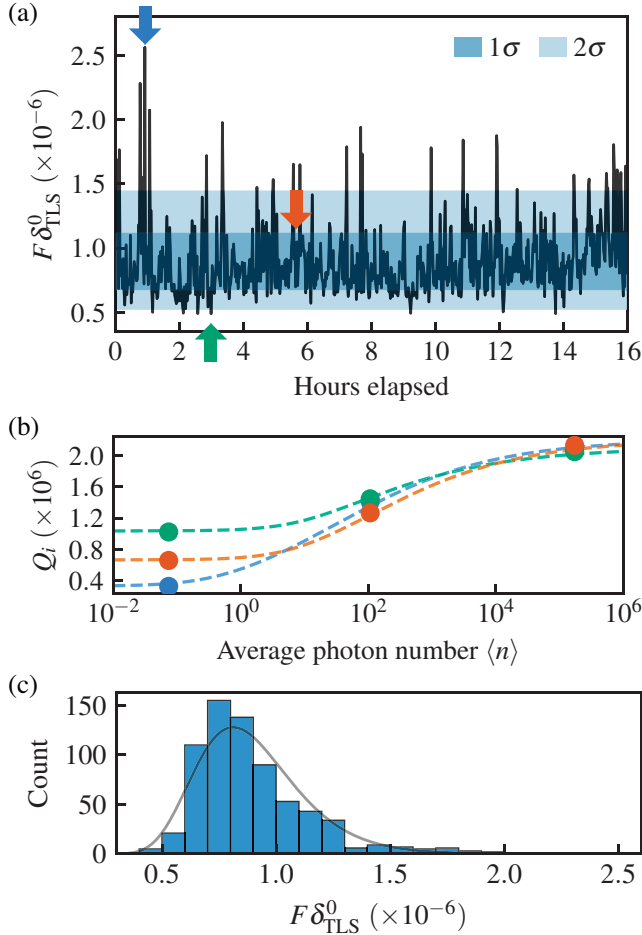


FIG. 3. Fluctuations of the effective TLS loss tangent $F\delta_{\text{TLS}}^0$. (a) Effective TLS loss tangent over 16 hours estimated from interleaved LP and HP measurements as $F\delta_{\text{TLS}}^0 \simeq 1/Q_{\text{LP}} - 1/Q_{\text{HP}}$. (b) Quality factors at LP, MP and HP, taken at instances of time shown by the arrows of the corresponding colors in (a). This illustrates how the TLS loss model curve varies over time, with the dashed lines being approximate fits to Eq. (2) to serve as guides to the eye. (c) Distribution of $F\delta_{\text{TLS}}^0$ for the data shown in (a), demonstrating the large spread in loss tangent. We obtain the 1σ and 2σ regions shown in (a) (shaded in blue) by fitting the histogram to a log-normal distribution (solid line).

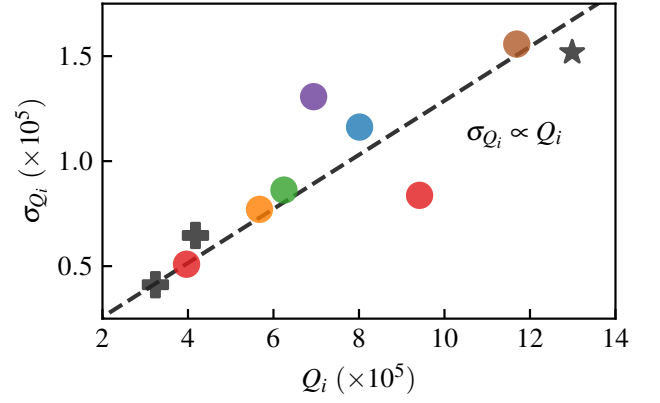


FIG. 4. Standard deviation of the internal quality factor σ_{Q_i} versus the average value at low power for various resonators. Our measurements results are shown as circles, where each color corresponds to a different device. The plus (star) signs are values obtained from Ref. 21 (Ref. 33). These results agree well with a linear model $\sigma_{Q_i} \propto Q_i$ (dashed line) obtained from considering an uniform TLS density of states with fluctuating couplings to the resonator²⁹. From it, we obtain an average standard deviation of $\sigma_{Q_i}/Q_i \simeq 13\%$.

In that case, performing a series of measurements as described here would provide the distribution width.

The distribution of the TLS loss tangent may additionally inform our understanding of relaxation time T_1 in superconducting qubits dominated by TLS loss. Indeed, near-resonant TLS are known to cause recurring periods of strong relaxation, appearing as telegraphic dynamics in a T_1 time trace^{22,24,32}. Tuning the qubit frequency away from these features, the T_1 background is characterized by a near-Gaussian distribution of higher coherence. We hypothesize that, beyond decoherence caused by coupling to individual near-resonant TLS, the fluctuations in TLS loss tangent observed in this work may contribute to variations in the background T_1 in superconducting qubits.

To further elucidate our results, we compare the standard deviation of Q_i with the mean value for low power measurements performed over several hours. We present results for various resonators measured over many cooldowns in addition to including results from other works^{21,33} (see Fig. 4). This illustrates that large fluctuations of the quality factor of superconducting resonators at low power appear to be universal across many devices. We observe good agreement with the linear relation $\sigma_{Q_i} \propto Q_i$. This is motivated by the use of an admittance model²⁹ that assumes a uniform TLS density of states with fluctuating couplings to the resonator. From it, we obtain relative fluctuations of $\sigma_{Q_i}/Q_i \simeq 13\%$. We note that the proportionality constant is power-dependent: fitting a linear model to high power measurements (Appendix H) similarly yields a reasonable agreement, with $\sigma_{Q_i}/Q_i \simeq 0.5\%$. The measurements in Fig. 4 were performed at similar but not identical low power levels, potentially explaining some deviations from the linear model.

In conclusion, we present results showing large internal

quality factor fluctuations for distributed-element superconducting microwave resonators. These fluctuations are observed across resonators, chips and cooldowns. The variations in internal quality factor can be linked to fluctuations in the loss tangent induced by two-level systems in the device materials. We find that the mean and standard deviation of Q_i obey a linear relationship. We demonstrate that performing time-averaged measurements over a few hours represents well the TLS loss tangent mean, while the standard deviation of the distribution is larger than the time-averaged fit uncertainty. Future work may help shed more light on the impact of different designs and materials and include the development of theoretical models to quantitatively explain our results. Further, we hypothesize that the TLS loss tangent fluctuations seen in this work are present in superconducting qubits as well. Future investigations may help identify a link between these fluctuations and the low-frequency background T_1 fluctuations observed in superconducting qubits dominated by TLS loss.

ACKNOWLEDGEMENTS

We would like to thank NIST ERB reviewers Mark Keller, Adam Sirois, and Eva Gurra for valuable feedback. This material is based upon work supported by the U.S. Department of Energy, Office of Science, National Quantum Information Science Research Centers, Superconducting Quantum Materials and Systems Center (SQMS) under contract no. DE-AC02-07CH11359.

AUTHOR DECLARATIONS

Conflict of Interest

The authors have no conflicts to disclose.

Author Contributions

André Vallières: conceptualization (lead); data curation (lead); formal analysis (lead); investigation (lead); methodology (lead); visualization (lead); writing - original draft preparation (lead); writing - review & editing (lead). **Megan E. Russell:** conceptualization (supporting); formal analysis (supporting); methodology (supporting); writing - original draft preparation (supporting); writing - review & editing (supporting). **Xinyuan You:** formal analysis (supporting); methodology (supporting); writing - review & editing (supporting). **David A. Garcia-Wetten:** resources (equal); writing - review & editing (supporting). **Dominic P. Goronzy:** resources (equal); writing - review & editing (supporting). **Mitchell J. Walker:** resources (equal); writing - review & editing (supporting). **Michael J. Bedzyk:** funding acquisition (supporting); supervision (supporting); writing - review & editing (supporting). **Mark C. Hersam:** funding acquisition (lead); supervision (supporting); writing - review & editing (supporting).

(supporting). **Alexander Romanenko:** supervision (supporting); writing - review & editing (supporting). **Yao Lu:** methodology (supporting); writing - review & editing (supporting). **Anna Grassellino:** funding acquisition (lead); supervision (supporting); writing - review & editing (supporting). **Jens Koch:** funding acquisition (lead); methodology (supporting); supervision (lead); writing - review & editing (supporting). **Corey Rae H. McRae:** conceptualization (supporting); formal analysis (supporting); methodology (supporting); supervision (lead); writing - original draft preparation (supporting); writing - review & editing (supporting).

Data Availability Statement

The data that support the findings of this study are available from the corresponding author upon reasonable request.

REFERENCES

- 1A. Blais, R.-S. Huang, A. Wallraff, S. M. Girvin, and R. J. Schoelkopf, *Physical Review A* **69**, 062320 (2004).
- 2A. Wallraff, D. I. Schuster, A. Blais, L. Frunzio, J. Majer, S. Kumar, S. M. Girvin, and R. J. Schoelkopf, *Nature* **431**, 162–167 (2004).
- 3M. Hofheinz, H. Wang, M. Ansmann, R. C. Bialczak, E. Lucero, M. Neeley, A. D. O. Connell, D. Sank, J. Wenner, J. M. Martinis, and A. N. Cleland, *Nature* **459**, 546–549 (2009).
- 4B. Mazin, *Microwave kinetic inductance detectors*, Ph.D. thesis (2004).
- 5J. M. Martinis, K. B. Cooper, R. McDermott, M. Steffen, M. Ansmann, K. D. Osborn, K. Cicak, S. Oh, D. P. Pappas, R. W. Simmonds, and C. C. Yu, *Physical Review Letters* **95**, 210503 (2005).
- 6W. Woods, G. Calusine, A. Melville, A. Sevi, E. Golden, D. Kim, D. Rosenberg, J. Yoder, and W. Oliver, *Physical Review Applied* **12**, 014012 (2019).
- 7D. P. Pappas, M. R. Vissers, D. S. Wisbey, J. S. Kline, and J. Gao, *IEEE Transactions on Applied Superconductivity* **21**, 871–874 (2011).
- 8A. Dunsworth, R. Barends, Y. Chen, Z. Chen, B. Chiaro, A. Fowler, B. Foxen, E. Jeffrey, J. Kelly, P. V. Klimov, E. Lucero, J. Y. Mutus, M. Neeley, C. Neill, C. Quintana, P. Roushan, D. Sank, A. Vainsencher, J. Wenner, T. C. White, H. Neven, J. M. Martinis, and A. Megrant, *Applied Physics Letters* **112**, 063502 (2018).
- 9C. R. H. McRae, R. E. Lake, J. L. Long, M. Bal, X. Wu, B. Juddersuren, T. H. Metcalf, X. Liu, and D. P. Pappas, *Applied Physics Letters* **116**, 194003 (2020).
- 10C. Müller, J. H. Cole, and J. Lisenfeld, *Reports on Progress in Physics* **82**, 124501 (2019).
- 11C. R. H. McRae, H. Wang, J. Gao, M. Vissers, T. Brecht, A. Dunsworth, D. Pappas, and J. Mutus, *Review of Scientific Instruments* **91**, 091101 (2020).
- 12K. D. Crowley, R. A. McLellan, A. Dutta, N. Shumiya, A. P. M. Place, X. H. Le, Y. Gang, T. Madhavan, M. P. Bland, R. Chang, N. Khedkar, Y. C. Feng, E. A. Umbarkar, X. Gui, L. V. H. Rodgers, Y. Jia, M. M. Feldman, S. A. Lyon, M. Liu, R. J. Cava, A. A. Houck, and N. P. de Leon, *Physical Review X* **13**, 041005 (2023).
- 13J. Gao, J. Zmuidzinas, B. A. Mazin, H. G. LeDuc, and P. K. Day, *Applied Physics Letters* **90**, 102507 (2007).
- 14S. Kumar, J. Gao, J. Zmuidzinas, B. A. Mazin, H. G. LeDuc, and P. K. Day, *Applied Physics Letters* **92**, 123503 (2008).
- 15R. Barends, H. L. Hortensius, T. Zijlstra, J. J. A. Baselmans, S. J. C. Yates, J. R. Gao, and T. M. Klapwijk, *IEEE Transactions on Applied Superconductivity* **19**, 936–939 (2009).
- 16T. Lindström, J. Burnett, M. Oxborrow, and A. Y. Tzalenchuk, *Review of Scientific Instruments* **82**, 104706 (2011).

- ¹⁷J. Gao, L. R. Vale, J. A. B. Mates, D. R. Schmidt, G. C. Hilton, K. D. Irwin, F. Mallet, M. A. Castellanos-Beltran, K. W. Lehnert, J. Zmuidzinas, and H. G. Leduc, [Applied Physics Letters](#) **98**, 232508 (2011).
- ¹⁸S. E. De Graaf, L. Faoro, J. Burnett, A. A. Adamyan, A. Y. Tzalenchuk, S. E. Kubatkin, T. Lindström, and A. V. Danilov, [Nature Communications](#) **9**, 1143 (2018).
- ¹⁹J. Burnett, A. Bengtsson, D. Niepce, and J. Bylander, [Journal of Physics: Conference Series](#) **969**, 012131 (2018).
- ²⁰D. Niepce, J. J. Burnett, M. Kudra, J. H. Cole, and J. Bylander, [Science Advances](#) **7**, eabh0462 (2021).
- ²¹J. Béjanin, Y. Ayadi, X. Xu, C. Zhu, H. Mohebbi, and M. Mariantoni, [Physical Review Applied](#) **18**, 034009 (2022).
- ²²P. Klimov, J. Kelly, Z. Chen, M. Neeley, A. Megrant, B. Burkett, R. Barends, K. Arya, B. Chiaro, Y. Chen, A. Dunsworth, A. Fowler, B. Foxen, C. Gidney, M. Giustina, R. Graff, T. Huang, E. Jeffrey, E. Lucero, J. Mutus, O. Naaman, C. Neill, C. Quintana, P. Roushan, D. Sank, A. Vainsencher, J. Wenner, T. White, S. Boixo, R. Babbush, V. Smelyanskiy, H. Neven, and J. Martinis, [Physical Review Letters](#) **121**, 090502 (2018).
- ²³J. J. Burnett, A. Bengtsson, M. Scigliuzzo, D. Niepce, M. Kudra, P. Delsing, and J. Bylander, [npj Quantum Information](#) **5**, 54 (2019).
- ²⁴J. H. Béjanin, C. T. Earnest, A. S. Sharafeldin, and M. Mariantoni, [Physical Review B](#) **104**, 094106 (2021).
- ²⁵M. Carroll, S. Rosenblatt, P. Jurcevic, I. Lauer, and A. Kandala, [npj Quantum Information](#) **8**, 132 (2022).
- ²⁶S. Zhu, X. You, U. Alyanak, M. Bal, F. Crisa, S. Garattoni, A. Lunin, R. Pilipenko, A. Murthy, A. Romanenko, and A. Grassellino, (2024), [arXiv:2409.09926](#).
- ²⁷M. S. Khalil, M. J. A. Stoutimore, F. C. Wellstood, and K. D. Osborn, [Journal of Applied Physics](#) **111**, 054510 (2012).
- ²⁸P. G. Baity, C. Maclean, V. Seferai, J. Bronstein, Y. Shu, T. Hemakumara, and M. Weides, [Physical Review Research](#) **6**, 013329 (2024).
- ²⁹C. Neill, A. Megrant, R. Barends, Y. Chen, B. Chiaro, J. Kelly, J. Y. Mutus, P. J. J. O'Malley, D. Sank, J. Wenner, T. C. White, Y. Yin, A. N. Cleland, and J. M. Martinis, [Applied Physics Letters](#) **103**, 072601 (2013).
- ³⁰J. Gao, *The Physics of Superconducting Microwave Resonators*, Ph.D. thesis, California Institute of Technology (2008).
- ³¹We used the `welch` function of the `scipy.signal` module in Python, applying a Hann window of length corresponding to 20% of the total trace length, 16,384 FFT samples and no detrending. The cross-spectral density is obtained using the `csd` function.
- ³²S. Schlör, J. Lisenfeld, C. Müller, A. Bilmes, A. Schneider, D. P. Pappas, A. V. Ustinov, and M. Weides, [Physical Review Letters](#) **123**, 190502 (2019).
- ³³C. T. Earnest, J. H. Béjanin, T. G. McConkey, E. A. Peters, A. Korinek, H. Yuan, and M. Mariantoni, [Superconductor Science and Technology](#) **31**, 125013 (2018).
- ³⁴C. J. Kopas, E. Lachman, C. R. H. McRae, Y. Mohan, J. Y. Mutus, A. Nersisyan, and A. Poudel, (2022), [arXiv:2204.07202](#).

Appendix A: Chip design

Our coplanar waveguide resonator chips are based on that described in Ref. 34. Room temperature, sputter deposited Nb films on Si (001) and (111) were patterned into the coplanar waveguide resonators with optical lithography and SF₆-based reactive ion etching. Each die is $7.5 \times 7.5 \text{ mm}^2$ and consists of eight, inductively coupled, quarter-wavelength resonators in the 4 GHz to 8 GHz range with target coupling quality factor of 5×10^5 to be close to critical coupling. An example chip design is shown in Fig. A.1. The dies were rigidly fixed to Au-plated Cu packages with two small dots of GE varnish on each corner, and ground plane and transmission line bonds (not shown) were made using aluminum wedge bonding.

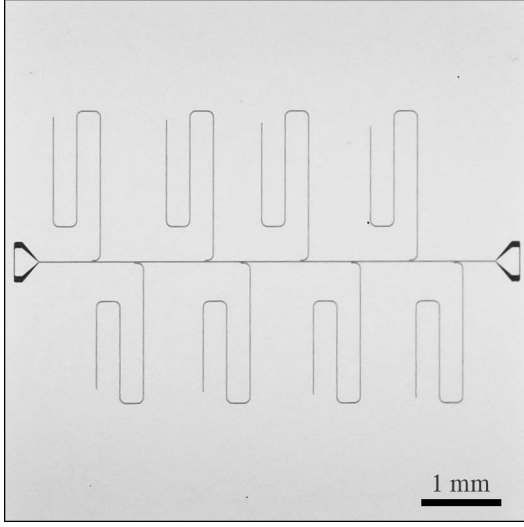


FIG. A.1. Photograph of a sample chip consisting of eight inductively-coupled quarter-wavelength superconducting resonators.

Appendix B: Measurement setup

Our measurement setup is shown in Fig. A.2. The input signal to the sample is first attenuated by a total of 70 dB and filtered through a 8 GHz low-pass filter then a commercial Eccosorb infrared (IR) filter. The output signal is amplified back using a JPA anchored at the mixing chamber stage ($\sim 10 \text{ mK}$), a high-electron mobility transistor (HEMT) amplifier at the 4 K stage, and a room-temperature amplifier, with isolators and filters along the line to minimize noise coming back to the sample. We operate our JPA by tuning its frequency using a current source and pumping at roughly twice the signal frequency using an external microwave signal generator. Additionally, we are able to measure multiple samples in the cooldown by using cryogenic switches and sharing the input/output lines (not shown in schematic).

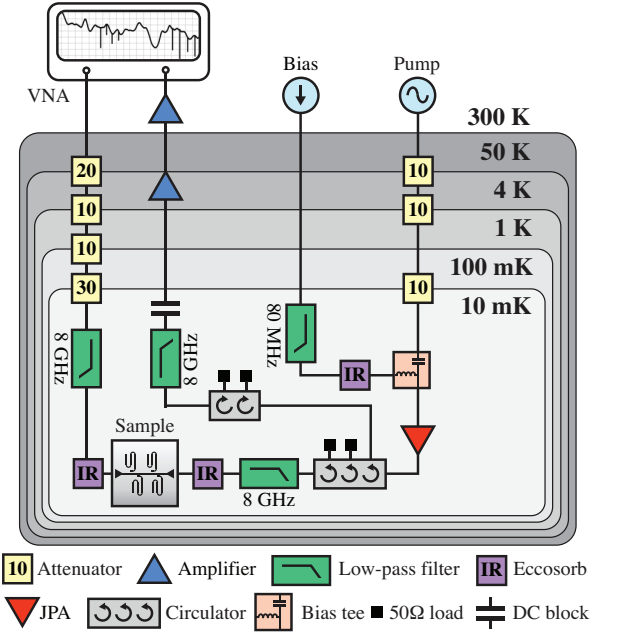


FIG. A.2. Wiring diagram for superconducting microwave resonators measurements. We use a VNA to probe our samples in the 4 GHz to 8 GHz range and a combination of microwave components to attenuate signals below single-photon level and amplify them back above noise level at room temperature.

Appendix C: Power dependence of f_{res} and Γ_i fluctuations

As most of the prior work focused on resonance frequency (f_r) and internal decay rate ($\Gamma_i = 2\pi f_r/Q_i$) fluctuations, in Fig. A.3 we show the noise spectra for these two variables at different powers, normalized to their average, computed as

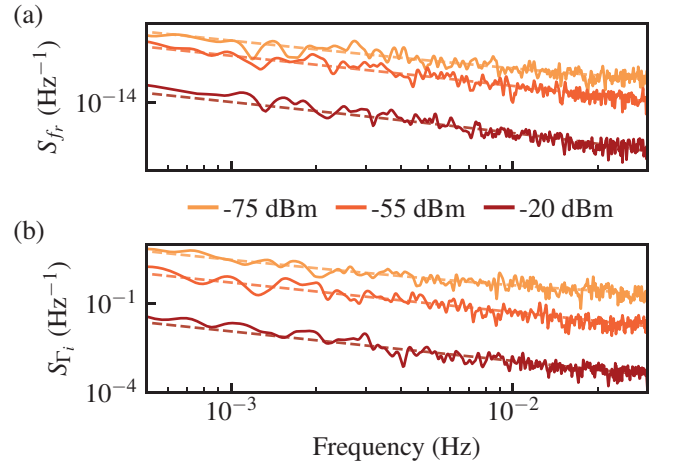


FIG. A.3. (a) Frequency and (b) decay rate noise spectra for various powers, where the legend refers to the power at the VNA. Fluctuations decrease with increasing power over the full range of frequencies, consistent with TLS saturation. The dashed lines are fits to a $1/f$ spectrum as guides to the eye.

explained in the main text using Welch's method. In agreement with these works, we see a decrease of the fluctuations for increasing power, with S_{Γ_i} being very similar to S_{Q_i} due to the large difference in fluctuation magnitude between Q_i and f_r .

Appendix D: Added noise due to the JPA

Since we use the JPA only at lower powers to achieve reasonable measurement rates, we must verify that the increased fluctuations at lower power is not caused by the amplification and that the JPA does not significantly increase Q_i noise. To do so, in Fig. A.4, we compare the internal quality factor noise spectrum with and without the use of the JPA at medium power obtained using Welch's method with the same parameters as in the main text. We see that the only notable difference is that the noise floor is lower when the JPA is on as the amplification brings the signal above the white noise level at these frequencies, as expected. In the $1/f$ region, where fluctuations are mainly caused by TLS, the spectra are basically the same and we can conclude that using the JPA does not negatively impact the measurements.

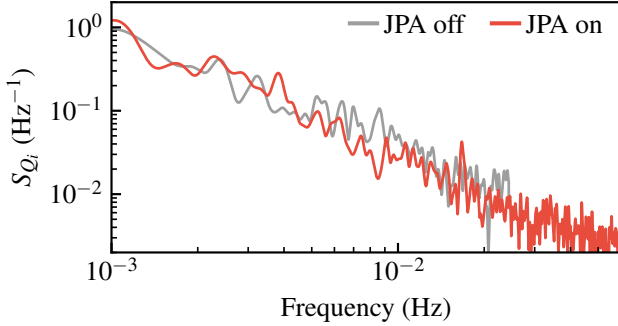


FIG. A.4. Internal quality factor noise spectra for measurements taken with and without the JPA. Each measurement was performed over 6 hours with measurement rates of 7 s and 21 s per sample, with and without the JPA respectively. The difference is negligible and could not cause the large fluctuations observed at low power.

Appendix E: Interleaved frequency measurement correlation

To confirm that the fluctuations are not due to the measurement setup, but rather from local noise to the resonators, in Fig. A.5, we show the signal coherence of two traces taken from interleaved measurement between two resonators. For each resonator, A and B , we first compute the normalized signal $(Q_i - \langle Q_i \rangle) / \langle Q_i \rangle$, where $\langle Q_i \rangle$ corresponds to the average value³¹. Then, using Welch's method as explained in the main text, we compute the signal coherence as $|S_{AB}|^2 / S_{AA} S_{BB}$, where S_{AB} is the cross spectral density, and S_{AA} or S_{BB} the spectral densities for resonators A and B . We observe a low correlation, indicating that the fluctuations are localized to the

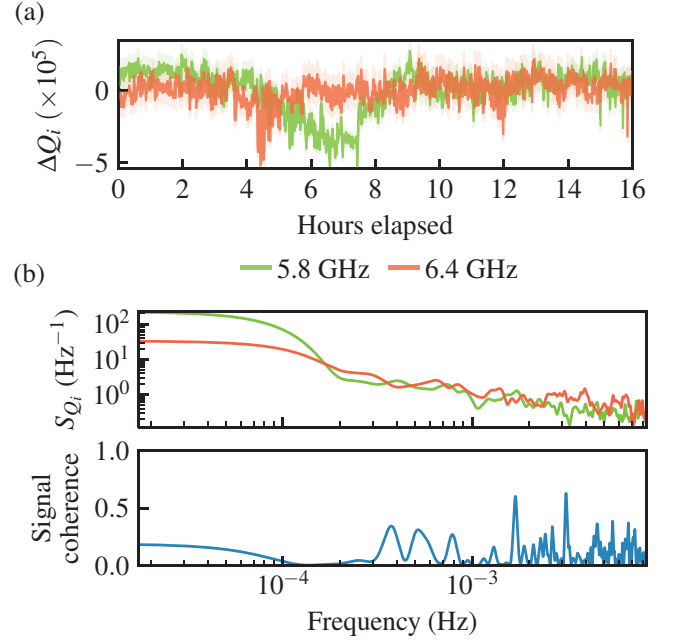


FIG. A.5. Interleaved resonator measurements of the internal quality factor over 16 hours with 30 s per point. (a) Time traces of the deviation from the average $\Delta Q_i = Q_i - \langle Q_i \rangle$ for the two resonators at 5.8 GHz and 6.4 GHz. The measurements were performed at medium power (-55 dBm at the VNA). (b) Internal quality factor noise spectra and signal coherence of the two resonators. The small signal coherence suggests that the fluctuations are local to each resonator.

resonators rather than being shared, as would be expected if they were due to amplifier noise, for example.

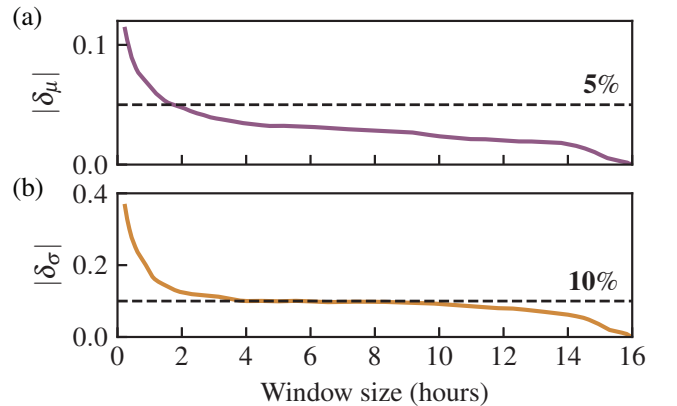


FIG. A.6. Deviation of the sample distribution parameters for the TLS loss tangent from their 16-hour values, as a function of window size. From the difference in mean δ_μ and standard deviation δ_σ , we observe that measuring over a few hours is necessary to achieve a target accuracy of 5% for the mean and 10% for the standard deviation.

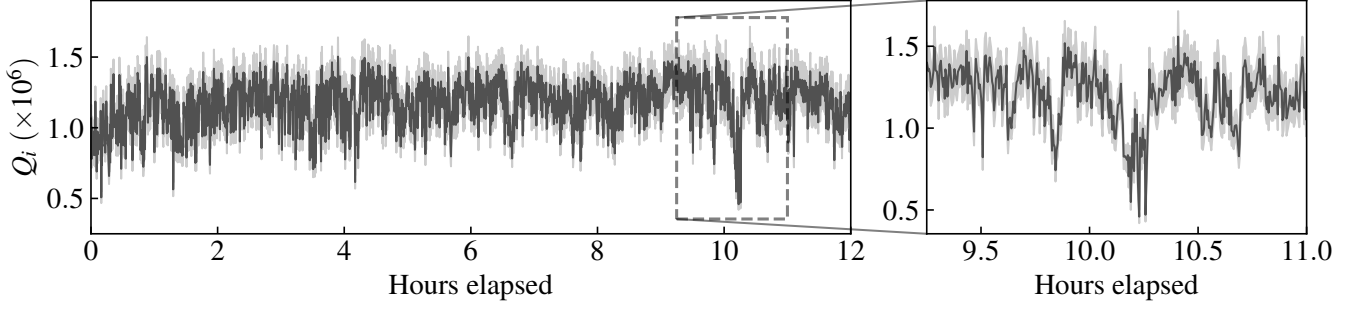


FIG. A.7. Full time trace of the internal quality factor at low power. The zoomed-in region shows a significant drop of over 70% from the maximum to minimum value in under 2 hours. The semi-transparent bands represent fitting uncertainty.

Appendix F: TLS loss tangent distribution over time

We have seen that the effective TLS loss tangent, $F\delta_{\text{TLS}}^0$ follows a log-normal distribution, and can be modeled by an average μ and standard deviation σ . By investigating how these parameters change as we increase the measurement time, we can estimate for how long low power measurements should be performed to obtain the TLS loss tangent with reasonable accuracy. In Fig. A.6, we show the average absolute difference between μ and σ per window size and their values for the full measurement time (i.e., 16 hours), denoted as $\delta_\mu = \mu - \mu_{16h}$ and $\delta_\sigma = \sigma - \sigma_{16h}$. For a target accuracy of 5% in the mean (10% in the standard deviation), we see that μ converges after about 2 hours, whereas for σ it takes twice as long. From these results, we recommend measurements over a few hours at low power to obtain the mean and standard deviation of the TLS loss tangent to within reasonable accuracy.

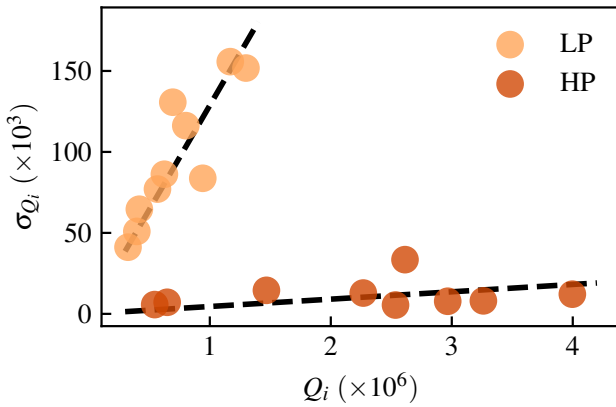


FIG. A.8. Standard deviation of the internal quality factor σ_{Q_i} versus the average value at high (HP) and (LP) powers for various resonators. The dashed lines are fits to a linear model $\sigma_{Q_i} \propto Q_i$, from which we obtain average fluctuations of 0.5% (13%) for measurements at high (low) power.

Appendix G: Sample full time trace

In Fig. A.7, we show a full 12-hour time trace of the internal quality factor at low power with a zoomed-in region of approximately 2 hours. We observe both slow and fast fluctuations, with occasional variations exceeding 50% in under 30 minutes, as illustrated on the right. These observations further demonstrate the need for extended measurements to accurately capture low-power Q_i due to significant fluctuations.

Appendix H: Linear trend in high power fluctuations

To further exemplify how the magnitude of fluctuations not only depend on Q_i but additionally on the power, in Fig. A.8, we have added high power measurements data to Fig. 4 in the main text, where measurements were taken over many hours, for different resonators and cooldowns. Fitting to a linear model, we observe an acceptable agreement and obtain a relative standard deviation of 0.5%. As for the low power data, we expect deviations from the linear model to originate from points being at different level of TLS saturation. Nevertheless, this suggests that as the number of photons in the resonator varies, the relation between σ_{Q_i} and Q_i stays roughly linear and can be useful in estimating fluctuations magnitude for a pair of power and Q_i .

Appendix I: Investigation of Q_c stability

As explained in the main text, all reported measurements of Q_i are obtained from fits to Eq. (1), from which we also obtain the coupling quality factor, Q_c . As this value is fixed for a given resonator, confirming that it does not vary significantly over time helps validating our measurement procedure. The average uncertainty and standard deviation of Q_c in Fig. A.9 are both around 2%. There is also little correlation between Q_i and Q_c , further confirming that the observed fluctuations in Q_i are not artificially induced by issues with fitting.

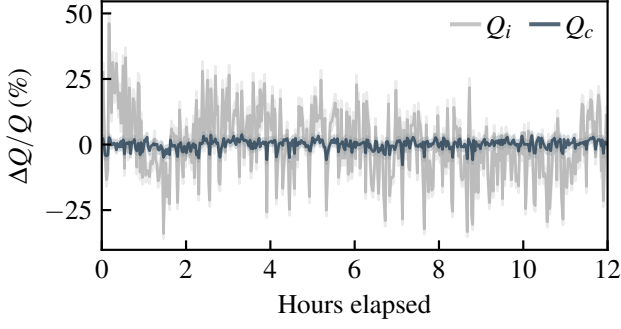


FIG. A.9. Relative change of the internal (Q_i) and coupling (Q_c) quality factors with respect to their average over time, showing that Q_c is stable in time. The semi-transparent bands represent fitting uncertainty.

Appendix J: Impact of measurement rate on the $F\delta_{\text{TLS}}^0$ distribution

$F\delta_{\text{TLS}}^0$ is well described by a log-normal distribution when averaging time is short as in this study, but due to the central limit theorem, the distribution necessarily evolves into a more symmetric distribution as averaging time increases. This effect could potentially explain the discrepancy between the near-Gaussian background T_1 distribution in superconducting transmon qubits²² and the log-normal distribution we observe in resonator TLS loss tangent. In Fig. A.10, we use measurements of the internal quality factor at low power Q_{LP} over 12 hours, sampled every 16 s, to construct the dataset shown. Indeed, by averaging consecutive samples, we simulate averaging over longer times, up to an averaging time of $\Delta t \simeq 25$ minutes for 91 samples. By averaging the high power intrinsic quality factor Q_{HP} from prior measurements, we can estimate the effective TLS loss tangent as $F\delta_{\text{TLS}}^0 \simeq 1/Q_{\text{LP}} - 1/Q_{\text{HP}}$ and visualize its distribution as a function of averaging time. The metric we use for normality testing is the skewness Z score computed using `scipy.stats.skewtest` function, which measures the symmetry of the distribution.

We note that at short averaging times the distribution is skewed, and progressively evolves into a more symmetric shape as averaging time increases. This is expected from the central limit theorem, where we can even predict the skewness to decrease as $1/\sqrt{\Delta t}$, although it does not describe the full behavior observed such as the apparent jump at $\Delta t = 10$ minutes. Nevertheless, we notice that the initial decrease in Z score plateaus at around $\Delta t = 2$ minutes, indicating that fast enough measurements of the loss can capture short mo-

ments of lower Q_i . This suggests that the T_1 background in superconducting qubits may look more skewed if sampled at a faster rate assuming the underlying physical mechanisms for fluctuations are similar.

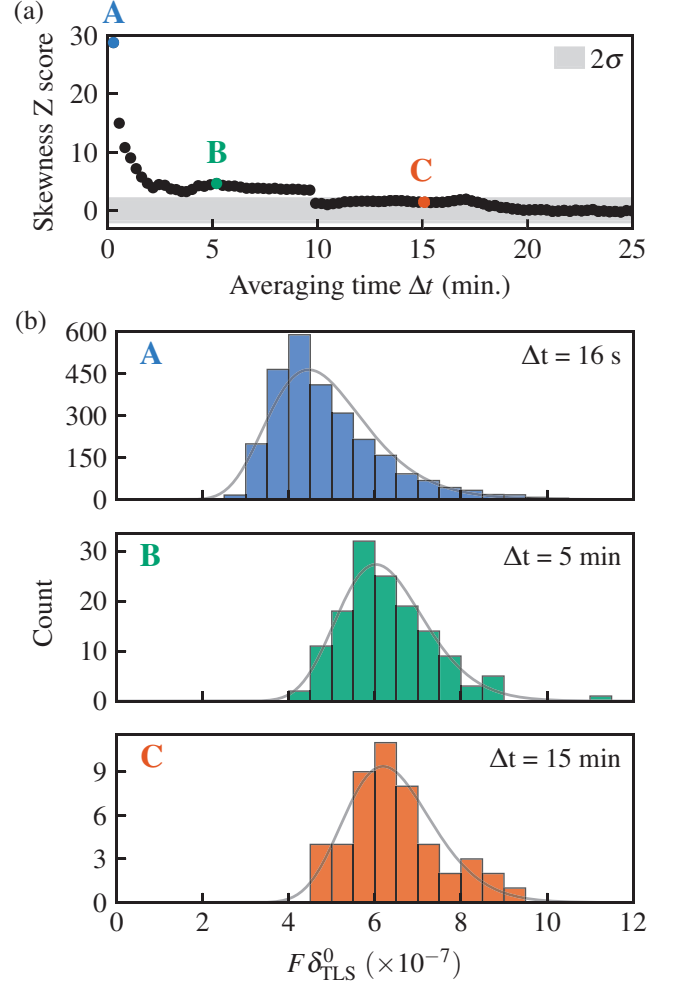


FIG. A.10. Statistical distribution of $F\delta_{\text{TLS}}^0$ versus averaging time, for a total measurement time of 12 hours. Datasets of various averaging time are constructed by averaging the raw VNA traces and fitting the results to Eq. (1). From this, we obtain the low power intrinsic quality factor Q_{LP} and estimate the effective TLS loss tangent as $F\delta_{\text{TLS}}^0 \simeq 1/Q_{\text{LP}} - 1/Q_{\text{HP}}$, with the high-power intrinsic quality factor Q_{HP} obtained from prior measurements. (a) The skewness Z score is used as a metric of the normality of the distribution and is shown to progressively converge towards zero. The 95% confidence interval is shown by the gray 2σ band ($Z = \pm 2$). (b) TLS loss tangent distributions at points A, B, and C, as shown in (a). The gray curves correspond to fits to a log-normal distribution.